

Sustainable Electronics Based on Crop Plant Extracts
and Graphene: A “Bioadvantaged” Approach

Original

Sustainable Electronics Based on Crop Plant Extracts

and Graphene: A “Bioadvantaged” Approach / Cataldi, Pietro; Heredia-Guerrero, José A.; Guzman-Puyol, Susana; Ceseracciu, Luca; La Notte, Luca; Reale, Andrea; Ren, Jun; Zhang, Yijie; Liu, Lei; Miscuglio, Mario; Savi, Patrizia; Piazza, Simonluca; Duocastella, Marti; Perotto, Giovanni; Athanassiou, Athanassia; Bayer, and Ilker S.. - In: ADVANCED SUSTAINABLE SYSTEMS. - ISSN 2366-7486. - ELETTRONICO. - (2018), pp. 1-11.

[10.1002/adsu.201800069]

Availability:

This version is available at: 11583/2711775 since: 2020-01-30T21:09:28Z

Publisher:

Weinheim : Wiley-VCH

Published

DOI:10.1002/adsu.201800069

Terms of use:

This article is made available under terms and conditions as specified in the corresponding bibliographic description in the repository

Publisher copyright

(Article begins on next page)

Sustainable Electronics Based on Crop Plant Extracts and Graphene: A “Bioadvantaged” Approach

Pietro Cataldi,* José A. Heredia-Guerrero, Susana Guzman-Puyol, Luca Ceseracciu, Luca La Notte, Andrea Reale, Jun Ren, Yijie Zhang, Lei Liu, Mario Miscuglio, Patrizia Savi, Simonluca Piazza, Marti Duocastella, Giovanni Perotto, Athanassia Athanassiou, and Ilker S. Bayer*

In today's fast-paced and well-connected world, consumer electronics are evolving rapidly. As a result, the amount of discarded electronic devices is becoming a major health and environmental concern. The rapid expansion of flexible electronics has the potential to transform consumer electronic devices from rigid phones and tablets to robust wearable devices. This means increased use of plastics in consumer electronics and the potential to generate more persistent plastic waste for the environment. Hence, today, the need for flexible biodegradable electronics is at the forefront of minimizing the mounting pile of global electronic waste. A “bioadvantaged” approach to develop a biodegradable, flexible, and application-adaptable electronic components based on crop components and graphene is reported. More specifically, by combining zein, a corn-derived protein, and aleuritic acid, a major monomer of tomato cuticles and sheellac, along with graphene, biocomposite conductors having low electrical resistance ($\approx 10 \Omega \text{ sq}^{-1}$) with exceptional mechanical and fatigue resilience are fabricated. Further, a number of high-performance electronic applications, such as THz electromagnetic shielding, flexible GHz antenna construction, and flexible solar cell electrode, are demonstrated. Excellent performance results are measured from each application comparable to conventional nondegrading counterparts, thus paving the way for the concept of “plant-e-tronics” towards sustainability.


1. Introduction

The tremendous increase in demand for consumer electronics^[1,2] constitutes a serious problem for the environment as these devices are discarded and replaced very frequently by the users.^[3,4] Estimates indicate that about 50 million tons of electronic waste or e-waste will be produced in 2018.^[5] Moreover, new-generation flexible plastic electronic materials, such as the ones used in wearable electronics or as sensors, will also be part of the plastic waste problem once they are discarded.^[6] Many of them contain non-biodegradable plastics, or toxic heavy metals and halogenated compounds.^[4,5,7] Efficient management and recycling of e-waste need to be encouraged and regulated but also more biodegradable and nature-derived materials should be integrated into consumer electronics in pursuit of sustainability.^[4,8,9] Although promising high-performance green devices have been recently demonstrated,^[7] a number of drawbacks associated with the use of

Dr. P. Cataldi, Dr. J. A. Heredia-Guerrero, Dr. S. Guzman-Puyol,
Dr. G. Perotto, Dr. A. Athanassiou, Dr. I. S. Bayer
Smart Materials
Istituto Italiano di Tecnologia
Via Morego 30, 16163 Genova, Italy
E-mail: pietro.cataldi@iit.it; ilker.bayer@iit.it

Dr. L. Ceseracciu
Materials Characterization Facility
Istituto Italiano di Tecnologia
Via Morego 30, 16163 Genova, Italy

Dr. L. La Notte, Prof. A. Reale
Department of Electronic Engineering
CHOSE (Centre for Hybrid and Organic Solar Energy)
University of Rome Tor Vergata
via del Politecnico 1, 00133 Rome, Italy

 The ORCID identification number(s) for the author(s) of this article can be found under <https://doi.org/10.1002/adsu.201800069>.

J. Ren, Y. Zhang, Prof. L. Liu
Department of Electrical Engineering
University of Notre Dame
Notre Dame, IN 46556, USA

Dr. M. Miscuglio
Optoelectronics Group
Istituto Italiano di Tecnologia
Via Morego 30, 16163 Genova, Italy

Prof. P. Savi
Department of Electronics and Telecommunication
Politecnico di Torino
Corso Duca degli Abruzzi 24, 10129 Torino, Italy

Dr. S. Piazza, Dr. M. Duocastella
Nanoscopy
Istituto Italiano di Tecnologia
Via Morego 30, 16163 Genova, Italy

DOI: 10.1002/adsu.201800069

plant or nature-derived soft materials, such as biodegradable polymers, exist, such as inferior physicochemical and thermo-mechanical properties compared to oil-based polymers that are particularly required to design robust, flexible, and conformal portable plastic electronic components.^[7,10,11] However, these drawbacks can be addressed steadily with continuous research and development efforts on green electronics by using various natural materials or precursors.^[3,12,13] For instance, electron transfer through proteins is essential for many biochemical reactions and, recently, proteins have been demonstrated to function effectively in electronic devices.^[14]

Today, green electronics is mostly associated with functionalization of cellulose fibers or nanocellulose with conductive nanoparticles,^[15–18] and in many cases, this involves interfacing cellulose surfaces with metal-based and/or inorganic nanomaterials.^[12,15,16,19] Hence, cellulose and conductive additives should have strong physicochemical interactions to maintain high-performance electronic output.^[17,20] Moreover, various biopolymers derived from plants or other natural processes, such as fermentation, have been successfully integrated into cellulose along with nanostructured carbon materials, such as nanotubes or graphene, to produce mechanically resistant flexible conductors.^[18,21] Even though cellulose-based electronic materials are very promising for green electronics, crop or domesticated plants produce and contain other potentially attractive renewable proteins and polymers^[22] and direct utilization of these resources in green electronics should be pursued as well. Biodegradable polymers are still considerably more expensive than oil-based polymers due to many multi-step polymerization and purification steps involved in their synthesis.^[23] In fact, this aspect has been recently addressed by Hernández et al.^[23] as a battle between “bioadvantage” and “bioreplacement”. In other words, the term bioreplacement refers to the collaboration between synthetic biology (engineering metabolic bacteria processes) and catalysis to obtain monomers from sugars and lignocellulosic feedstocks that can subsequently be used to produce bio-polyesters, and also some conventional polymers we know today such as butadiene, isoprene, and styrene.^[23] The “bioadvantage” strategy, however, exploits the multifunctional precursors or components given to us by nature combined in simple but novel ways to yield new polymers/composites with attractive properties. In general, this approach has the potential to be much more cost-effective compared to “bioreplacement.” The present study follows the latter approach towards developing high-performance sustainable flexible electronics using plant extracts without further processing and the concept is envisioned as a real plant-based electronics or plant-*e*-tronics.

Certain plant proteins such as zein^[24,25] or plant cuticles^[26] can be easily extracted from crops and may be directly used in tandem to produce alternative and cost-effective green electronic components. Corn-derived zein is a prolamine protein widespread in bakery products^[27,28] and in food packaging/safety applications.^[27,29] Zein can be processed into films either by melting or in alkaline aqueous or alcohol solutions. Its films are very rigid and brittle requiring plasticizers for flexibility.^[30] Instead, plant cuticle such as tomato skin contains useful waterproof aliphatic polyester networks of hydroxylated fatty acids known as cutin.^[26,31] Among them, aleuritic acid (9,10,16-trihydroxyhexadecanoic acid) can be thermally polymerized into

polyaleuritate, a cutin-like polyester,^[32] having good waterproof and barrier properties as well as full biodegradability.^[33] It is also the main component of resinous lac named shellac that is secreted on tree branches and leaves by certain insects.

Herein, we investigated electrical performance and electronic applications of flexible biodegradable conductors produced by dispersing graphene nano-platelets (GnPs) in a zein–polyaleuritate matrix that is embedded in a cellulose fiber support. The cellulose fiber support ensures that the resulting biomaterial is flexible^[34] and mechanically stable under severe folding and twisting conditions. Zein, aleuritic acid, and GnPs were dispersed in an organic solvent and the resulting ink was spray-coated on both sides of a pure cellulose membrane. The coated membrane was hot-pressed at temperatures^[26] sufficient to in situ polymerize aleuritic acid resulting in a flexible composite. We also show that in situ formed polyaleuritate binds zein with the cellulose, mimicking the composite plant cell wall composition (protein, polysaccharides, and hydroxyl fatty acids).^[35] The developed biocomposites biodegrade in seawater under dark. Various high-performance electronic applications of these folding- and twisting-resistant green conductors were demonstrated such as sub-millimeter (microwave) electromagnetic interference (EMI; 500–750 GHz) shielding, efficient GHz antennas adaptable to Wi-Fi applications, and flexible electrode for organic photovoltaics.

2. Results and Discussion

The first challenge we faced in this work, in order to be able to combine components of different chemistry from different plant crops, was to find a common solvent to co-solubilize these plant elements. We found that an equal volume mixture of methanol/chloroform that is a common protein extraction liquid from plants^[36] dissolves both zein and aleuritic acid at high concentrations. Before dispersing GnPs in the solutions, the combined plant extract concentration in the ink formulation was optimized as 0.017 g mL⁻¹ zein and 0.013 g mL⁻¹ aleuritic acid. GnP concentrations were added to tune electrical properties from 0.1 to 40.0 wt% with respect to dry weight polymer content. Characteristics of the GnPs were presented in our earlier report^[37] (see also Figure S1 (Supporting Information) for Raman details). The physicochemical and mechanical characteristics of the cellulose substrate were also given in our previous publications.^[18] The schematic in **Figure 1a** demonstrates the steps of the fabrication process of the final composite biomaterial. The conductive ink was first spray-coated on both sides of the cellulose membrane and, after solvent evaporation, the composite was hot-pressed at 190 °C (20 min) in order to infiltrate the blend inside the fiber network^[18,21,38] and at the same time to form polyaleuritate in situ (see chemical characterization performed with Fourier transformed infrared spectroscopy (FTIR) in Figure S2, Supporting Information).^[26] During polymerization, the polyester acted as a strong compatibilizer between zein and cellulose as shown in Figure S2 (Supporting Information). Using thermogravimetric analysis (TGA), we ensured that none of the natural materials underwent thermal degradation due to hot-pressing conditions (see Figure S3, Supporting Information). Indeed, the hot-pressing procedure was performed at 190 °C and thermal degradation

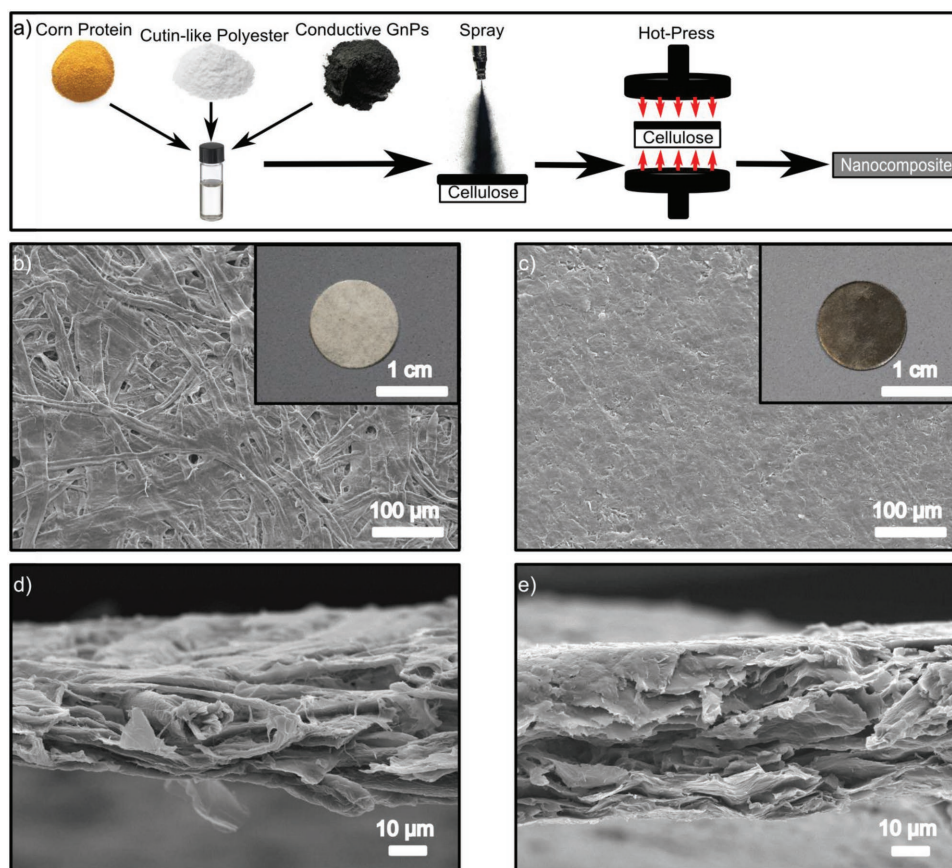


Figure 1. a) A schematic of the preparation of the plant-based conductive material. From left to right, conductive ink preparation, spray-coating, and hot-pressing-assisted impregnation. b) SEM images of the morphology of the bare cellulose network with the relative photograph in the inset. c) SEM topography of the GnPs-bio-based nanocomposite with the relative photograph as an inset. d,e) SEM cross sections of the cellulose fiber network and of the conductor GnPs-plant modified, respectively.

started after 200 °C. Micromorphology of the pristine cellulose membrane resembles unsized paper with an approximate fiber diameter of 10–20 μm (Figure 1b). Once the graphene biocomposite is hot-pressed into the bulk of the membrane, a black “graphene paper” forms as shown in the inset of Figure 1c, and its surface micromorphology (Figure 1c) resembles a homogeneous amorphous thermoplastic–GnP composite surface structure.^[39] The comparison of the cross-sectional micromorphology of the cellulose membrane and the biocomposite in Figure 1d,e indicates that the impregnation does not create a thick layer (both thickness are about 40 μm) but rather embeds all the materials of the ink into the cellulose membrane bulk interlaces.

In order to determine the minimum amount of GnPs needed to impart electrical conductivity to the biocomposites,^[18,40] a percolation study^[21,38,41,42] was conducted as shown in **Figure 2a** as a plot of the sheet resistance versus GnPs concentration, in terms of GnPs weight percent with respect to the combined weight of zein and polyaleuritate. The electrical percolation threshold was observed at around 5 wt% GnPs concentration, where the sheet resistance sharply declined from 10^8 to 10^4 – 10^3 Ω sq⁻¹ levels. Nonetheless, the biocomposite can sustain much higher concentrations of GnPs (30–40 wt% or approximately 20–30 wt% with respect to the final weight of

the biocomposite, cellulose included) reaching nearly 10 Ω sq⁻¹ sheet resistance levels without losing its flexibility and resistance to severe repeated twisting and folding events.

The electromechanical properties of the most conductive biocomposite (30 wt%) were characterized under multiple loop-twist cycles (repetitive twisting events). Such tests simulate torsion, one of the most common stresses experienced by a flexible material.^[43] Experiments were conducted for 100 cycles of twist–untwist events (this experiment is provided in Video S1, Supporting Information). The ratio of the instantaneous resistance to the initial resistance (R_i/R_0), plotted in Figure 2b, was found to oscillate around 1 with a maximum amplitude of approximately 4% of the R_0 . This value remains well within the experimental measurement error that was recorded as $\pm 10\%$ of the mean value. Increasing the number of twist–untwist cycles beyond 100 did not induce any further increase in the maximum oscillation range of 4%. A demonstration of this remarkable resistance to twisting events is given as insets in Figure 2b with further evidence shown in Video S2 (Supporting Information). Indeed, three light-emitting diodes (LEDs) were uninterruptedly powered at a voltage of 12 V with the biocomposite undergoing several twist–untwist events without any loss in brightness. To confirm the mechanical robustness of the biocomposites, multiple 180° folding–unfolding experiments were

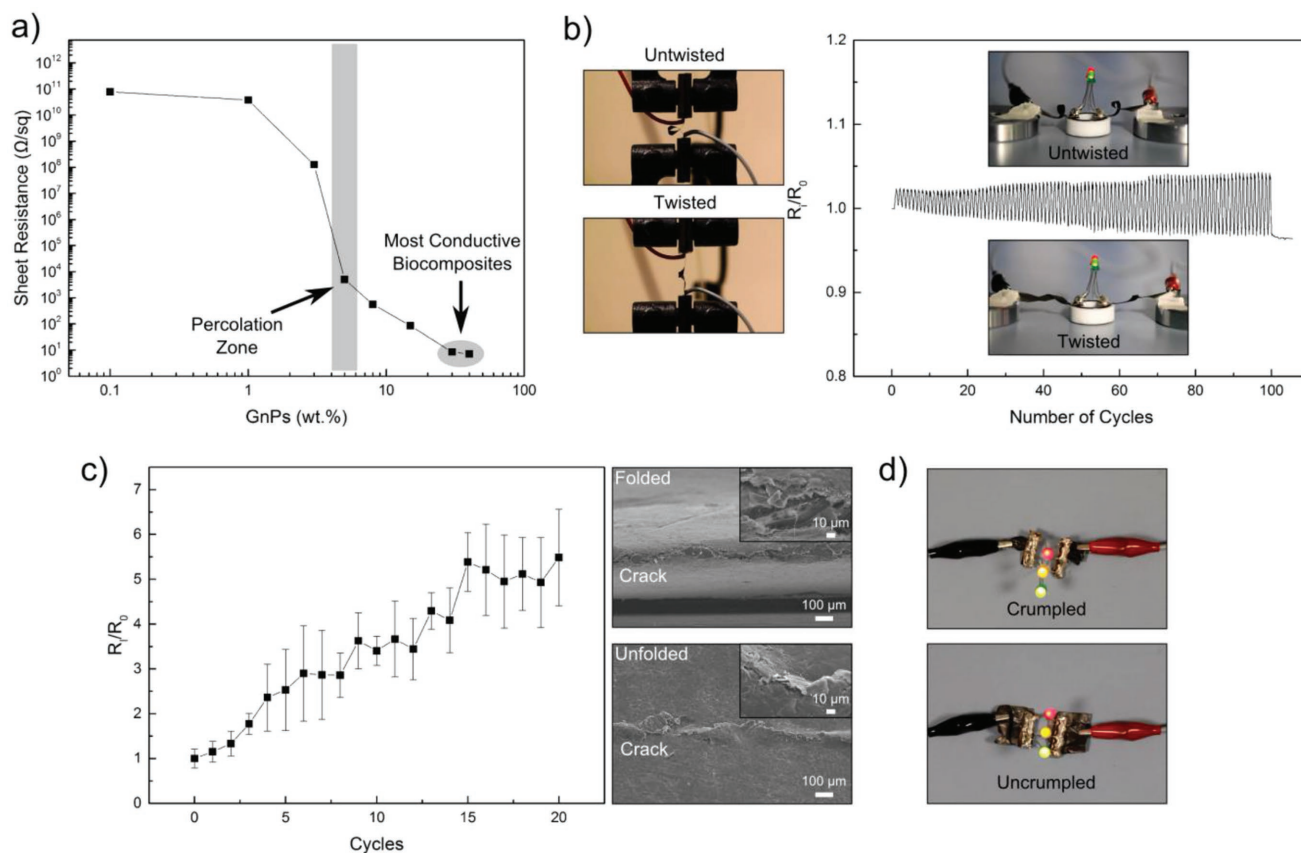


Figure 2. a) Electrical percolation threshold of the plant-nanocomposites as a function of GnPs concentration. b) Twisting stability of electrical conductivity on the 30 wt% GnPs sample. On the left, photograph of the experimental setup. On the right, normalized resistance variation with increasing number of cycles. c) Changes in normalized resistance (R_i/R_0) as a function of folding–unfolding cycles. A 2 kg weight was run over the fold mark. The SEM images show the folded and unfolded regions after 20 cycles. d) Photographs demonstrate robustness of the biocomposite powering an LED even when crumpled into a ball.

also conducted.^[18] Commonly, such kind of tests are completed without causing complete bending and without enforcing a permanent fold mark.^[20,44] Instead, to induce further severity in each fold–unfold events, the fold line was pressed with a 2 kg weight.^[18,21,38] The variation in R_i/R_0 across the fold mark for 20 weight-pressed fold–unfold cycles is reported in Figure 2c. After the first 15 cycles, the resistance increased by roughly a factor of five, after which it stabilized. As mentioned earlier, the initial average sheet resistance was approximately $10 \Omega \text{ sq}^{-1}$, and after 20 folding cycles, it settled around $50 \Omega \text{ sq}^{-1}$. Although a five-fold increase is evident, the final sheet resistance is comparable or better than other reported carbon-based flexible conductors^[45–47] or non-carbon-based conductors undergoing similar fatigue tests,^[48,49] which are not based on “bioadvantaged” plant-based resources (see Table S1, Supporting Information, for more details). Scanning electron microscopy (SEM) images shown in Figure 2c demonstrate the micromorphology of the formed fold mark or the crack at the end of the experiments. Although the fold line (crack) is obvious, it is not in the form of a deep crack or fully separated micro-valley but rather in the form of a superficial discontinuity or a roughness alteration. This suggests that many connected GnPs are still present within the depth of the fold mark that can maintain ohmic electric conductivity after the 20th cycle.^[18,21] The biocomposite

resilience was also demonstrated by crumpling it into a “paper ball” state repeatedly, which did not hamper its ability to light up 12 V powered LEDs (see Figure 2d; Video S3, Supporting Information). All in all, such promising fatigue resistance results hint at the emergence of rather robust electromechanical properties once the cellulose membrane was impregnated with the “bioadvantaged” ink. Particularly, the stiffness and flexibility of the biocomposites were similar to those of cellulose. Detailed mechanical characterization results are given in Figure S4 (Supporting Information). Indeed, the nanocomposites and the cellulose paper exhibit similar Young modulus, elongation at break, and ultimate strength. Furthermore, the biocomposites demonstrate superior heat dissipation properties compared to the cellulose membrane (Figure S5, Supporting Information).

Graphene and graphene oxide are known to biodegrade in the presence of enzymes and in aqueous environment containing physiological peroxide levels.^[50,51] However, the fate of graphene or graphene oxide in lakes, rivers, or oceans is still under investigation.^[50,51] We have investigated the biodegradation potential of the most conductive biocomposite using a standard biochemical oxygen demand (BOD) test while also monitoring sample weight loss in seawater (Genoa area, Italy) under dark condition for one-month duration. This test is by no means an evidence of full biodegradation but suggests the

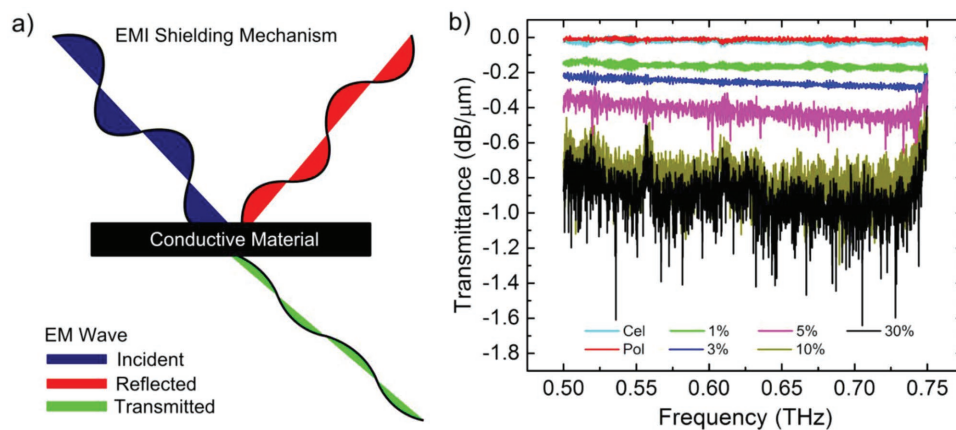


Figure 3. a) Schematic of the EMI shielding mechanism. b) Terahertz EMI shielding characteristics of the biocomposites in terms of frequency-dependent transmittance. *Cel* and *Pol* are the pure cellulose and the fibrous substrate modified with zein and AC, respectively. The values indicated in percentage correspond to the amount of GNPs of the samples.

potential of the material to biodegrade. The results and the relevant quantitative discussion are given in Figure S6 (Supporting Information). In summary, the degradation of the biocomposite was initiated after 6 days in dark seawater, and after 24 days, the oxygen consumption rate reached $87 \text{ mg O}_2 \text{ L}^{-1}$ that is considered as a substantial biodegradation rate.^[52] Note that the overall GNP content of the most conductive biocomposite is 30 wt% including the weight of the cellulose membrane and our measurements cannot distinguish if a certain portion of the GNPs also contribute to the oxygen consumption (i.e., they also biodegrade). Hence, we can argue that under the experimental conditions herein (local sea water kept in dark), the oxygen consumption rate originates from the degradation of organic constituents (i.e., zein, polyaleuritate, and cellulose).

The convergence of cellulose-like mechanical properties, excellent electrical conductivity, use of “bioadvantaged” materials, biodegradability, enhanced thermal characteristics, lightweight, and potential scalability in a single composite make the biocomposites very attractive platforms for various high-performance electronics applications. In the following, we demonstrate their suitability for such applications, like microwave EMI shielding performance, a flexible GHz antenna, and as an electrode for a flexible solar cell.

3. THz EMI Shielding

The EMI between closely packed electronic circuitry, devices, and instruments, triggered by widespread employment of alternating current, induces breakdown or malfunction of projected performance of electrical appliances.^[53] Consequently, effective and efficient electromagnetic (EM) screening is necessary to ensure the expected functioning of electronics apparatus (as, e.g., computers, smartphones, televisions, etc.).^[54] Such phenomenon is called EMI shielding. Practically, when an EM wave interacts with a conductive material, part of it is reflected, part is absorbed, and the residual part is transmitted as schematically shown in Figure 3a. The lower the amplitude of the transmitted wave is, the larger the EM screening. Typically, EMI shielding is obtained with metallic materials, which require

complicate micro- and nano-fabrication procedures.^[55] Recently, due to the exceptional combination of electrical, mechanical, thermal, and dielectric features of nanofiller-modified plastics, nanocomposites have been used for suppression of electromagnetic noise.^[21,56]

In light of its low sheet resistance ($\approx 10 \text{ } \Omega \text{ sq}^{-1}$), lightweight, and flexibility, the most conductive biocomposite developed in this work is an ideal candidate as sustainable EMI shielding attenuator. Considering the increasing speed of electronics appliances, high-frequency EMI shielding (i.e., THz) is gaining more and more importance in fields as diverse as security, optoelectronics, imaging, space science, and biological sensing.^[55,57,58] Therefore, these “bioadvantaged” green conductors could be exploited to substitute expensive, rigid, and corrosion-susceptible metallic conductors as THz shields, contributing to the rise of high-speed circuit applications built with safe components for the environment. The EMI shielding measurements were performed at frequencies between 0.5 and 0.75 THz for normal incidence (see Figure 3) on biocomposite samples with different GNPs concentrations. Losses in the incoming electromagnetic wave due to screening (also known as EMI shielding effectiveness (SE)) were calculated using $SE \text{ (dB)} = -10 \log(P_t/P_i)$, where P_t is the transmitted electromagnetic power and P_i is the incident power.^[55] The ratio P_t/P_i is called transmittance and is a function of the frequency of the incoming EM wave. In Figure 3b, the normalized EMI SE with respect to biocomposite thickness (i.e., the absolute value of the transmittance) as a function of the frequency of the incident EM waves is reported for samples with different GNP concentrations. Neither pure cellulose nor cellulose impregnated with the zein–polyaleuritate polymer blend demonstrated any electromagnetic shielding effect (0 dB) in the absence of GNPs. The SE reached approximately $0.8 \text{ dB } \mu\text{m}^{-1}$ for the biocomposite with 10 wt% GNPs concentration, and around $0.9 \text{ dB } \mu\text{m}^{-1}$ for the sample with 30 wt% GNPs. The obtained results closely approach some of the highest attenuation levels reported ($\approx 1 \text{ dB } \mu\text{m}^{-1}$) for other carbon-based nanocomposites in the literature,^[21,59] as reported in Table S2 (Supporting Information). The shielding effectiveness reported in this work achieves a value of $\approx 45 \text{ dB}$ (or normalized SE of $0.9 \text{ dB } \mu\text{m}^{-1}$) for the

50- μm -thick 30 wt% GnPs sample, significantly exceeding the threshold value of EMI SE required for commercial applications (i.e., 20 dB, or less than 1% transmittance of electromagnetic wave).^[60] Note that the measurement data for both the 10 and 30 wt% GnPs biocomposites show highly fluctuating signals due to the limited system dynamic range. In addition, the measured transmittance for the 10 and 30 wt% GnPs show peaks at 0.56 and 0.75 THz, respectively. This is generated by an additional reduction in dynamic range due to water absorption at those frequencies. Overall, the biocomposites offer high THz shielding performance, showing great potential to replace conventional metallic conductors as THz shielding materials.

4. GHz Antenna

Availability of flexible and sustainable antennas suitable for many different portable electronic devices is a key target to replace metals with lighter, cheaper, energy-efficient materials but also to reduce *e-waste* to a certain extent.^[2,61] Flexibility is becoming a major objective of next-generation compliant electronics including near-field communication.^[62,63] Antennas permit the reception and transmission of electromagnetic radio waves (3 kHz–300 GHz) and are indispensable in efficient wireless communication.^[61] The trend towards flexible and wearable electronics has promoted innovative applications for antennas in distinct technological fields, such as health monitoring,^[64] antennas for nonplanar and limited spaces,^[65] and reconfigurable antennas.^[66] Conformable antennas in the form of conductive metal-based geometries on flexible plastic substrates have been demonstrated.^[66,67] Herein, we demonstrate that our plant-*e*-tronic conductors can be laser-machined into desired or specific GHz antenna designs. As an example, the design of a commercially available Wi-Fi antenna (Figure 4a,b) was duplicated by laser-cutting the most conductive flexible biocomposite. The performance of the antenna was then measured in order to characterize different features and judge its suitability for a real electronic application (for details on characterization experiments, refer to Figure S7 (Supporting Information) and Materials and Methods sections). One of the most common characteristics used to describe the performance of an antenna is the scattering parameter or return loss or reflection coefficient designated as S11. When expressed in dB, it represents how much power is reflected from the antenna.^[68] If S11 = 0, the antenna does not function, since all the power is reflected and nothing is radiated. The return loss of both antennas (commercial and the plant-*e*-tronic) was measured with a network analyzer, as schematically shown in Figure 4b. Both antennas were placed on a flexible cardboard that served as a common dielectric background.

Figure 4c shows the return loss of the two antennas recorded in the frequency band 1–4 GHz. The measurement indicates that the commercial antenna (red solid line) resonates at 2.5 GHz with a return loss of –13 dB, and its characteristic –10 dB bandwidth is 0.45 GHz. The plant-*e*-tronic antenna (black solid line), instead, shows a resonance at 2.18 GHz, with a return loss of \approx –22 and –10 dB bandwidth of 0.54 GHz. As such, the plant-*e*-tronic antenna shows smaller reflection coefficient and wider operative bandwidth compared to the

commercial antenna. In other words, at its resonance, the power fed to the antenna is effectively radiated. The relatively small return loss of the plant-*e*-tronic antenna is a direct consequence of the low and stable sheet resistance.^[69] Note that the resonant frequency of such thin-film antennas strongly depends on the interaction of the conductive components of the antenna with the dielectric environment (air and the substrate or support)^[70] under which they are operated. This allows the designer to change and tune its resonance frequency by modifying the dielectric, conducting materials and geometry. Afterwards, we measured the radiation diagram in polar coordinates for the plant-*e*-tronic antenna. Such plots demonstrate antenna's radiation characteristics as a function of the incidence angle,^[71] as shown in Figure 4d,e. Figure S7 (Supporting Information) demonstrates the details of the measurement setup. The peaks (lobes) represent the distribution of power at different angles. The total gain pattern in the horizontal and vertical planes (H- and E-planes, respectively) highlights \approx 15 dB gain corresponding to the horn aperture (between 150° and 240°, 90° angle of aperture). The front-to-back ratio (see Figure 4e), which corresponds to the ratio of power gain between the front and rear of the fabricated antenna, is 4 dB (\approx 160% of directionality). The front-to-back ratio was shown to be in the same range as that of the commercial antenna (2.6 dB,^[72] \approx 135% of directionality) thus demonstrating its full functionality.

In summary, the plant-*e*-tronic antenna shows smaller reflection coefficient and wider operative bandwidth compared to the commercial antenna and it is approximately 20% more directional. This suitable radiofrequency performance makes these “bioadvantaged” plant-based conductors potential candidates for a wide variety of wireless applications, such as radiofrequency identification^[73] or high-speed communications.^[74] Note that due to inherent flexibility and mechanical resistance, the design and geometry of the biocomposite conductors can be easily modified according to desired frequency resonances suitable for wearable electronics applications.

5. Top Electrode for Flexible Photovoltaics

Photovoltaic devices are inspired by the photoinduced charge separation due to sunlight harvesting by plant photosynthesis.^[75,76] Plant leaves function as flexible, biodegradable, and lightweight solar energy harvesters and converters. Polymer solar cells (PSCs), compared to conventional silicon modules,^[77,78] have been developed to mimic natural leaf to exhibit some structural characteristics such as conformability, light weight per unit area, and all-organic constituents. Furthermore, the materials employed for PSCs are often solution-processable and of low cost.^[79–81] Among the possible solvent-assisted production methods, spray-coating possesses many advantages such as large area adaptation and the ability to coat both linear and curved substrates^[82,83] in short times. Thus, spray-manufactured PSCs are considered ideal for large-scale polymeric solar cell production.^[81] However, drawbacks still exist such as the non-eco-friendly nature of some of the materials employed.^[84,85] The ultimate goal would be to manufacture fully biodegrading highly efficient PSCs in a cost-effective way.

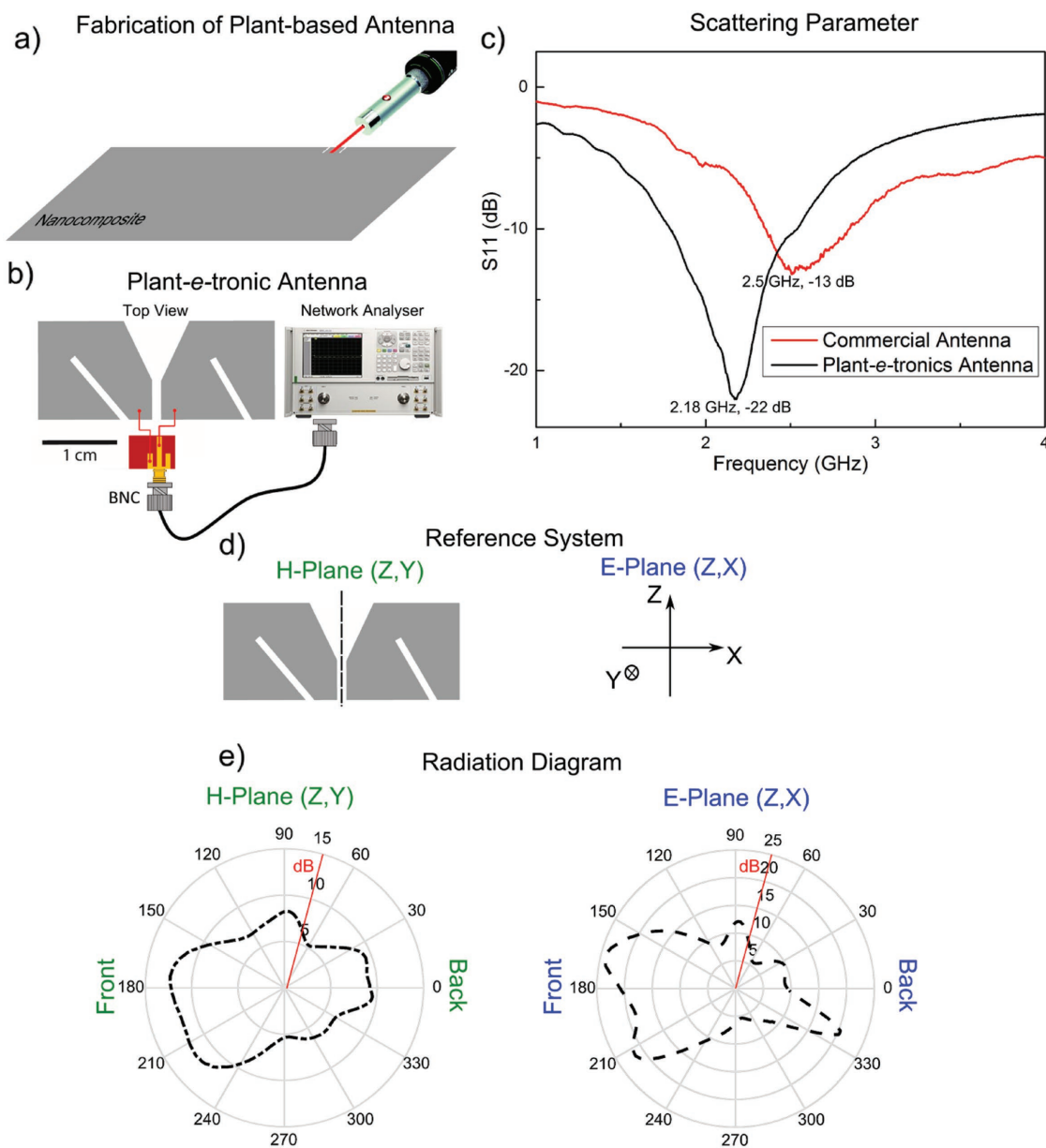


Figure 4. a) Scheme of the laser-cut fabrication of the conductive part of the antenna. b) Top view of the antenna and experimental setup. c) Measured return loss of the plant-e-tronic antenna and the commercial antenna. d) Reference system for the radiation pattern measurements. e) Radiation pattern of the plant antenna at 2.18 GHz in the H- and E-planes. The red solid line represents the dB scale.

With this in mind, the most conductive plant-e-tronic biocomposite was utilized as the top electrode of a fully sprayed PSC^[79] design, as schematically exhibited in **Figure 5a**. The biocomposite was laminated on top of a multilayer structure fabricated by spraying all the layers in air starting from a polyethylene terephthalate (PET) substrate coated with a three-layer ITO/Ag/ITO as transparent conductive bottom electrode.^[79] The active area of the flexible solar cell was 15 mm². An inverted configuration was chosen in light of its ease of scalability and compatibility with polymer:fullerene systems.^[86] First, a double layer composed of zinc oxide (ZnO; ≈20 nm thick) and polyethylenimine (PEIE; ≈10 nm thick) was sprayed as an electron transport and extraction system. This configuration had been

previously shown to improve the open circuit voltage (V_{OC}) and short circuit current (J_{SC}).^[79] The active layer was composed of a polythiophene polymer (PffBT4T-2OD) and PC₇₀BM fullerene. This system was employed since it forms highly crystalline and sufficiently pure small polymer domains that ensure robust morphology and excellent performance.^[87] Another advantage is the easy scalability due to the large thickness,^[82] thus facilitating the coating of large-area substrates, even with a rough and irregular surface. Vanadium oxide (V_2O_x) was sprayed onto PffBT4T-2OD:PC₇₀BM as hole transport layer, followed by the deposition of poly(3,4-ethylenedioxythiophene)polystyrene sulfonate)/D-sorbitol, which acts as an electronic glue between the sprayed stack and the final plant-nanocomposite. The overall

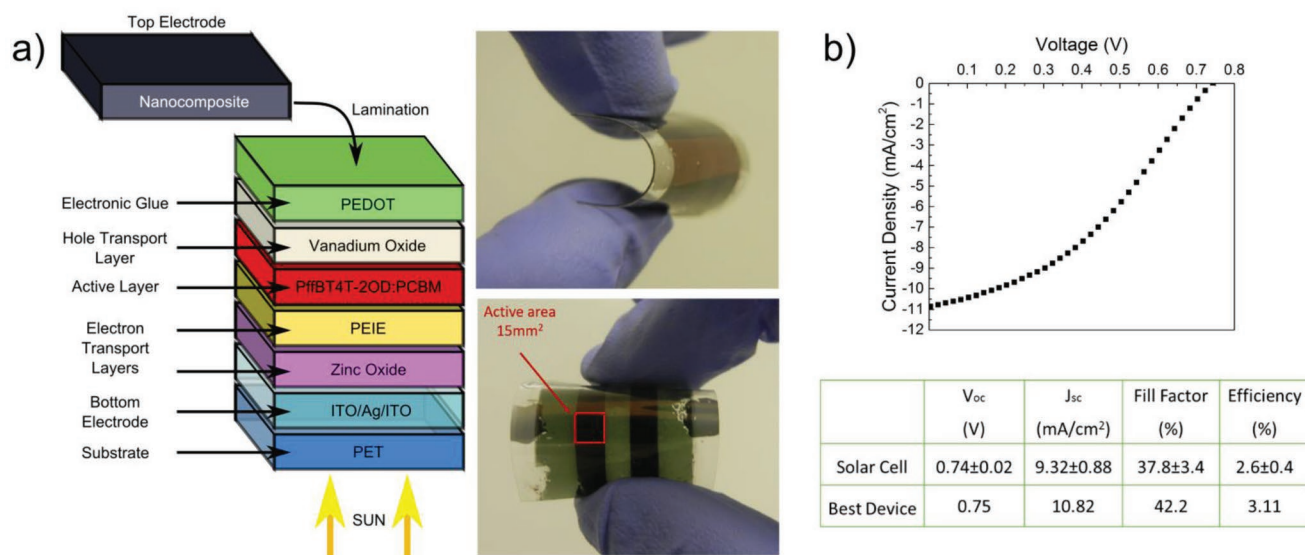


Figure 5. a) On the left: schematic of the multilayer structure of the fully sprayed PSC. On the right: photograph of the obtained devices. b) J - V characteristic of the best device and table with the resume of the electrical parameters of the photovoltaic cells (average values over 10 devices and standard deviations).

electrical parameters of the PSCs and the current–voltage (J - V) curve of the best device are displayed in Figure 5b. The average power conversion efficiency was measured to be 2.6% with a maximum value of 3.1%. These results are comparable with those obtained in our previous work where fully sprayed devices were made with a “bioreplacement” top electrode.^[79] This demonstrates that i) the biocomposite has a suitable value of sheet resistance for this application due to the favorable isotropic electrical conduction pathways among GnPs within the sample bulk morphology and ii) the electronic glue is compatible with the biocomposite by ensuring the physical adhesion needed for the vertical conduction. Even though the PSCs exhibit a relatively high V_{OC} , they show lower short circuit current density (J_{SC}) and fill factor compared to devices with standard evaporated top electrode.^[79] However, organic photovoltaic devices based on this biocomposite top electrode shows electrical performances significantly higher than other fully sprayed devices based on glass or fabrics.^[88,89] It can be concluded that “bioadvantaged” natural materials can also be integrated into flexible solar cell technologies and help the reduction of non-degrading polymeric elements in the manufacturing.

6. Conclusions

With the aim to advance towards next-generation sustainable flexible electronics, we have designed and developed a fully organic plant and graphene-based “bioadvantaged” flexible conductor for the first time. The fabrication method is very simple and straightforward and also adaptable to large area covering. The obtained biocomposite conductors feature low sheet resistance ($\approx 10 \Omega \text{ sq}^{-1}$), with excellent resilience against fatigue confirmed by repeated twisting and folding stability tests. We also proved biodegradability in dark sea waters with biochemical oxygen demand measurements. Next, we demonstrated

various high-performance electronic applications such as EMI shielding at THz frequencies, with attenuation levels exceeding 40 dB. Laser-cutting was employed to transform the biocomposites into a flexible GHz antenna design. The resulting antenna displayed smaller reflection coefficient and wider operative bandwidth in the GHz frequency region compared to a commercial Wi-Fi antenna, proving an effective radiation and power balance for GHz transmission. Finally, the biocomposites were utilized as the top electrode of a fully sprayed flexible PSC demonstrating promising power conversion efficiencies of over 3%. Hence, by combining the novel “bioadvantaged” plant-based conductor materials and their promising advanced electronics applications along with mechanical robustness, a new concept of plant-*e*-tronics was developed that can establish another step forward towards sustainable and portable electronics.

7. Experimental Section

Materials: Cellulose substrates/membranes ($\approx 30 \mu\text{m}$ thick) were purchased from Korff (Art. No. 60285). Zein was purchased from Sigma-Aldrich and used as received. Aleuritic acid (98% purity by NaOH titration) was acquired from TCI Europe. GnPs were donated by Directa Plus (grade Ultra G+); details on graphene thickness and lateral size can be found in an earlier report.^[37] Chloroform and methanol (analytical degree) were purchased from Sigma-Aldrich. Zein (0.5 g) and aleuritic acid (AC) (0.4 g) solutions were prepared in chloroform:methanol solution (1:1, v:v, total volume 30 mL). Different weight percent of GnPs were added for electrical percolation measurements and the solutions were homogenized with tip sonication (Sonics & Materials, Inc., Model No. VCX750, 750 W, 40% amplitude, 20 kHz, three times for 30 s). The maximum amount of GnPs employed was 0.012 g mL^{-1} for the 40 wt% GnPs-loaded sample. This concentration of GnPs was correspondent to approximately 1 wt% of GnPs relative to the amount of solvent employed. A 4 mL of the solution was spray-coated (2.0 bar, 15–18 cm distance, Paasche Air Brush, USA) on both sides of cellulose membrane rectangles (15 cm²) and the obtained composite was hot-pressed

(20 bar, Specac-Atlas Power Presses T8) for 20 min at a temperature of 190 °C to achieve impregnation of the ink and to polymerize aleuritic acid into polyaleuritate polyester.^[26] Teflon anti-stick films (Advent Research Material, Art. Num. FP823338) were used during the hot-pressing procedure to avoid sticking of the nanocomposites on the press platen.

Methods: LabRAM 600 spectrometer (maximum power 20 mW, diffraction grating of 600 lines per mm, excitation wavelength of 632.8 nm HeNe laser) was employed to measure Raman spectra. Infrared measurements of samples were obtained with an attenuated total reflectance (ATR) accessory (MIRacle ATR, PIKE Technologies) coupled to FTIR spectrometer (FT/IR-4100, JASCO). All spectra were recorded in the range from 3800 to 600 cm⁻¹ with 4 cm⁻¹ resolution, accumulating 128 scans. In a typical measurement, the sample was gently placed on the spot of the ATR accessory and slowly pressed. TGA of the specimens was done by means of a TA instruments machine (model Q500) in N₂ flow. SEM images were acquired through a JEOL microscope (model JSM-6490LA) operating at an acceleration voltage of 15 kV. The samples were stored at -195.79 °C in liquid nitrogen, and cut by tearing them with two tweezers so to preserve the original morphology while analyzing their cross section.

Biodegradability was evaluated through a standard BOD test by measuring the oxygen amount consumed during a month in a biodegradation reaction in water.^[90] For each sample, three measurements were collected and the results were averaged to obtain a mean value. Carefully weighed samples (≈200 mg) were finely minced and immersed in 432 mL bottles containing seawater collected from the Genoa (Italy) area shoreline. Oxygen consumed during the biodegradation process was recorded at different time intervals by using sealed OxyTop caps on each bottle which can assess the oxygen levels. BOD from blank bottles filled with only seawater was also measured for reference.

The electrical characteristics of samples with different GnP wt% were recorded determining the sheet resistance with a four-probe resistance system (Keithley 2611A sourcemeter). Silver paste electrodes (SPI Conductive Silver Paint, sheet resistance ≤0.01 Ω sq⁻¹) of 3 mm were painted on the samples, keeping apart 3 mm spacing. The susceptibility of electrical conduction of the material upon weak deformations was studied through loop-twist tests. Samples were clamped at both ends rotating one sample extreme of 180° relative to the other extreme, forming a loop. According to the topological conservation law,^[91,92] the sum of the writhe Wr (non-planarity of the ribbon axis) and of the twist Tw (turns around the ribbon axis) of an open curve is constant

$$Wr + Tw = const \quad (1)$$

In the initial configuration, these two parameters were $Wr = 1$ and $Tw = 0$. Increasing the clamp distance, the ribbon axis was aligned, so that Wr tends to 0 and Tw to 1. This means that upon clamp separation/closure, the samples configuration shifted cyclically from full writhe (tensile strain regime) to full twist (shear strain regime). The former configuration corresponds to a uniaxial strain $\epsilon_w = \frac{t}{2R}$, and the latter to a shear stress $\epsilon_t = \frac{\pi w}{L}$ (t = thickness = 0.04 mm, w = width = 4 mm, R = loop curvature = 1.5 mm, L = length = 20 mm). With a cyclic test (separation rate 5 mm min⁻¹, test duration 100 cycles), it is switched between the two configurations, thus simulating the complex and constantly shifting deformation of textile materials. Folding-unfolding cycles were implemented by measuring the resistance variation across the fold mark. A cylindrical weight of approximately 2 kg was passed on the folding edge during the folding cycle. A uniaxial testing machine (Instron 3365) was utilized to measure the mechanical properties of the nanocomposites and of the raw materials (initial length 25 mm, width 4 mm, deformation rate 1 mm min⁻¹). In order to determine the thicknesses of the different samples, a micrometer (Mitutoyo; series 293) was used. The EMI shielding measurements were performed using a WR-1.5 (0.50–0.75 THz) Vector Network Analyzer (VNA) system, i.e., a Keysight N5245A PNA in conjunction with two Virginia Diodes Inc. (VDI) WR-1.5 extenders. Measurements were done after turning

on the system for about an hour to reach a steady state. Two WR-1.5 horn antennas were employed at the ends of the two extenders to couple the electromagnetic wave (THz signal) to and from the air. The THz signal from the horn antenna of the first extender was reflected/collimated by a parabolic mirror to normally incident onto the plant-based biocomposite sample under test. The transmitted THz signal was then reflected/focused by another parabolic mirror onto the horn antenna of the second extender. The ratio of the received power to the incident one (or transmittance) characterizes the EMI SE of the sample. The measured transmittance was normalized to sample thickness for a fair comparison, as shown in Figure 3b. The thermal properties of pure cellulose and of the plant-nanocomposite with 30 wt% GnPs were investigated via IR-camera (FLIR A310) and using FLIR Researcher software for image analysis. The samples were placed on a hot plate (IKA, model C-MAGHP10) at 145 °C, kept at a distance of 0.6 cm from the hot surface (two rectangular cardboards were used as spacer). In this way, the samples were heated up by the convective heat transfer exerted by air. The range of the measurement was set between 40 °C and 90 °C. Video S4 (Supporting Information) shows one of the realized measures. All the tests described above were performed with minimum five samples, unless specified differently, and at 25 °C and 44% relative humidity (RH). Green, yellow, and red LEDs were purchased from LEDSupply (model L1-0-G5TH30-1, L1-0-Y5TH20-1, and L2-0-R5TH20-1, respectively) and mounted on copper plates. A tension of 12 V was applied to light them up.

Antenna Fabrication and Characterization: The homemade laser direct-writing system used to cut the nanocomposite substrate consisted of a Ti:sapphire amplifier (Coherent, Inc.) tuned at a wavelength of 800 nm, with a pulse duration of 100 fs. The laser pulse energy was controlled by two neutral density filters and a rotating $\lambda/2$ -waveplate. In order to achieve a through-cut of the substrate, the Gaussian beam at the output of the amplifier was shaped into a Bessel beam using an axicon lens (Plano-Convex Axicon, apex angle 178°, Altechna), and sent to the sample through a 4f system with a total demagnification of 25, with the last focusing lens being a 50X NA 0.55 objective lens (Plan Apo Infinity Corrected Long WD Objective, Mitutoyo, Inc.). Note that Bessel beams present an extended depth of field while maintaining a very small spot size, enabling the direct through-cut of materials without the need of axial focus control.^[93] The translation of the sample relative to the laser beam allowed the direct cutting of the nanocomposite with arbitrary shapes, such as the antenna reported herein. In more detail, an XYZ motorized stage (Prior Scientific, Inc.) was used for sample translation, and custom software, written in LabView language, was used to control and synchronize the laser unit with the stage displacement. For all the experiments, the laser energy per pulse was set to 100 μ J. Finally, direct inspection of the laser fabrication process was performed with a charge-coupled device (CCD) camera (DCC1645C, Thorlabs Inc.) coaxially placed with respect to the laser beam.

The reflection coefficient of the antennas was measured with a VNA (Agilent E8361A) after a standard one-port calibration (open/short/load). The commercial antenna was connected with a microcoaxial cable (50 Ω) as described in the datasheet,^[72] while the prototype was connected with a matched microstrip line. The measurements of the radiation pattern were performed in an anechoic chamber with a network analyzer (Agilent N5227A). The positioner of the antenna under test was moving on a spherical scanning (θ , ϕ). The probe antenna was a double-ridged horn (1–18 GHz) and the distance between the antenna under test and the probe was 2.7 m (see Figure S7, right panel, Supporting Information). A whole spherical scan of the antenna under test was performed with a step of 2° in θ and $\phi = 0^\circ$ and $\phi = 90^\circ$. The total gain radiation patterns were obtained by summing the two vectors measured E-pol and H-pol in the principal planes.

Flexible Photovoltaic Cell Fabrication: PET foils coated with a transparent conductive ITO/Ag/ITO multilayer (Solutia, ≈8 Ω sq⁻¹) were patterned by wet acidic etching and then cleaned by ultrasonic bath with detergent, water, and isopropanol. The spray deposition of the inks was performed under chemical hood by using a dual-action airbrush (Mecafer) supplied by compressed air with pressure set at 2 bar for all the layers. ZnO nanoparticles dispersion was purchased by

Sigma-Aldrich and diluted in 1:100 in ethanol. PEIE, 80% ethoxylated solution, from Sigma-Aldrich was dissolved in ethanol to get a concentration of 0.1 wt%. ZnO and PEIE solutions were deposited at substrate-nozzle distance = 10 cm, flow rate = 4 mL min⁻¹, and spraying time = 3 and 2 s, respectively. PffBT4T-2OD polymer and PC₇₀BM fullerene, both purchased from Cal-OS, Inc., were dissolved in 1:1.2 ratio in ortho-xylene to obtain a total concentration of 17.6 mg mL⁻¹ with a 3% v/v amount of 1,8-di-iodooctane. The active layer formulation was sprayed at substrate-nozzle distance = 5 cm, flow rate = 1 mL min⁻¹, and ink volume = 400 μL. V₂O₅ sol-gel prepared by dissolving 0.02 mL of vanadium (V) oxytriisopropoxide in 3 mL of 2-propanol was sprayed at substrate-nozzle distance = 10 cm, flow rate = 2 mL min⁻¹, spraying time = 3 s. The electronic glue was composed of Clevios F HC Solar:water in the ratio 1:1 and D-sorbitol with a concentration of 3.75% v/v. This formulation was sprayed at substrate-nozzle distance = 15 cm, flow rate = 4 mL min⁻¹, and ink volume = 2 mL. The plant-e-tronic nanocomposite was applied to the sprayed stack through lamination at 110 °C and 0.3 bar by using a flat-bed heat-press machine.

Supporting Information

Supporting Information is available from the Wiley Online Library or from the author.

Acknowledgements

The authors gratefully acknowledge Directa Plus S.p.a. for donating the graphene nanoplatelets. The authors also gratefully acknowledge Lara Marini and Matteo Bustreo for TGA and IR-camera support, respectively.

Conflict of Interest

The authors declare no conflict of interest.

Keywords

crops, flexible electronics, graphene, green electronics, sustainable electronics

Received: May 7, 2018
Revised: July 2, 2018
Published online:

- [1] H. N. Khan, D. A. Hounshell, E. R. Fuchs, *Nat. Electron.* **2018**, *1*, 14.
 [2] M. Irimia-Vladu, *Chem. Soc. Rev.* **2014**, *43*, 588.
 [3] M. Irimia-Vladu, E. D. Gowacki, G. Voss, S. Bauer, N. S. Sariciftci, *Mater Today* **2012**, *15*, 340.
 [4] M. J. Tan, C. Owh, P. L. Chee, A. K. K. Kyaw, D. Kai, X. J. Loh, *J. Mater. Chem. C* **2016**, *4*, 5531.
 [5] X. Zeng, C. Yang, J. F. Chiang, J. Li, *Sci. Total Environ.* **2017**, *575*, 1.
 [6] G. Khandelwal, A. Chandrasekhar, N. R. Alluri, V. Vivekananthan, N. P. M. J. Raj, S.-J. Kim, *Appl. Energy* **2018**, *219*, 338.
 [7] Y. H. Jung, T.-H. Chang, H. Zhang, C. Yao, Q. Zheng, V. W. Yang, H. Mi, M. Kim, S. J. Cho, D.-W. Park, H. Jiang, J. Lee, Y. Qiu, W. Zhou, Z. Cai, S. Gong, Z. Ma, *Nat. Commun.* **2015**, *6*, 7170.
 [8] Z. Zhang, M. Tsang, I.-W. Chen, *Nanoscale* **2016**, *8*, 32 15048.
 [9] S.-W. Hwang, J.-K. Song, X. Huang, H. Cheng, S.-K. Kang, B. H. Kim, J.-H. Kim, S. Yu, Y. Huang, J. A. Rogers, *Adv. Mater.* **2014**, *26*, 3905.
 [10] J. A. Rogers, Y. Huang, *Proc. Natl. Acad. Sci.* **2009**, *106*, 10875.
 [11] J. Bae, M. K. Song, Y. J. Park, J. M. Kim, M. Liu, Z. L. Wang, *Angew. Chem., Int. Ed.* **2011**, *50*, 1683.
 [12] M. Irimia-Vladu, N. S. Sariciftci, S. Bauer, *J. Mater. Chem.* **2011**, *21*, 1350.
 [13] G. Mattana, D. Briand, A. Marette, A. V. Quintero, N. F. de Rooij, *Org. Electron.* **2015**, *17*, 77.
 [14] I. Ron, L. Sepunaru, S. Itzhakov, T. Belenkova, N. Friedman, I. Pecht, M. Sheves, D. Cahen, *J. Am. Chem. Soc.* **2010**, *132*, 4131.
 [15] J. Lessing, A. C. Glavan, S. B. Walker, C. Keplinger, J. A. Lewis, G. M. Whitesides, *Adv. Mater.* **2014**, *26*, 4677.
 [16] M.-C. Hsieh, C. Kim, M. Nogi, K. Suganuma, *Nanoscale* **2013**, *5*, 9289.
 [17] D. Tobjörk, R. Österbacka, *Adv. Mater.* **2011**, *23*, 1935.
 [18] P. Cataldi, I. S. Bayer, F. Bonaccorso, V. Pellegrini, A. Athanassiou, R. Cingolani, *Adv. Electron. Mater.* **2015**, *1*, 12.
 [19] Y. Jo, S.-J. Oh, S. S. Lee, Y.-H. Seo, B.-H. Ryu, J. Moon, Y. Choi, S. Jeong, *J. Mater. Chem. C* **2014**, *2*, 9746.
 [20] A. Russo, B. Y. Ahn, J. J. Adams, E. B. Duoss, J. T. Bernhard, J. A. Lewis, *Adv. Mater.* **2011**, *23*, 3426.
 [21] P. Cataldi, F. Bonaccorso, A. E. del Rio Castillo, V. Pellegrini, Z. Jiang, L. Liu, N. Boccardo, M. Canepa, R. Cingolani, A. Athanassiou, I. S. Bayer, *Adv. Electron. Mater.* **2016**, *2*, 1600245.
 [22] J. B. Van Beilen, Y. Poirier, *Plant J.* **2008**, *54*, 684.
 [23] N. Hernández, R. C. Williams, E. W. Cochran, *Org. Biomol. Chem.* **2014**, *12*, 2834.
 [24] A. R. Flory, D. V. Requesens, S. P. Devaiah, K. T. Teoh, S. D. Mansfield, E. E. Hood, *BMC Biotechnol.* **2013**, *13*, 28.
 [25] J. A. Gwartz, M. N. Garcia-Casal, *Ann. N. Y. Acad. Sci.* **2014**, *1312*, 66.
 [26] J. A. Heredia-Guerrero, J. J. Bentez, P. Cataldi, U. C. Paul, M. Contardi, R. Cingolani, I. S. Bayer, A. Heredia, A. Athanassiou, *Adv. Sustainable Syst.* **2017**, *1*, 1.
 [27] G. Gorrasi, L. Vertuccio, *J. Cereal Sci.* **2016**, *70*, 66.
 [28] B. A. Bugusu, O. Campanella, B. R. Hamaker, *Cereal Chem.* **2001**, *78*, 31.
 [29] A. Yemenicioglu, *Antimicrobial Food Packaging*, Elsevier, Amsterdam **2016**, pp. 503–513.
 [30] J. W. Lawton, *Cereal Chem.* **2002**, *79*, 1.
 [31] J. J. Bentez, J. A. Heredia-Guerrero, S. Guzmán-Puyol, M. J. Barthel, E. Domnguez, A. Heredia, *Front. Mater.* **2015**, *2*, 59.
 [32] J. A. Heredia-Guerrero, A. Heredia, E. Domnguez, R. Cingolani, I. S. Bayer, A. Athanassiou, J. J. Bentez, *J. Exp. Bot.* **2017**, *68*, 5401.
 [33] J. J. Bentez, J. A. Heredia-Guerrero, M. I. de Vargas-Parody, M. A. Cruz-Carrillo, V. Morales-Flórez, N. de la Rosa-Fox, A. Heredia, *J. Phys. D: Appl. Phys.* **2016**, *49*, 175601.
 [34] I. Khan, K. Saeed, I. Khan, *Arabian J. Chem.* **2017**, *33*, 2017.
 [35] A. Heredia, A. Jiménez, R. Guillén, *Zeitschrift Lebensmittel-Untersuchung Forschung* **1995**, *200*, 24.
 [36] A. Vertommen, B. Panis, R. Swennen, S. C. Carpentier, *Planta* **2010**, *237*, 1113.
 [37] P. Cataldi, I. S. Bayer, G. Nanni, A. Athanassiou, F. Bonaccorso, V. Pellegrini, A. E. del Rio Castillo, F. Ricciardella, S. Artyukhin, M.-A. Tronche, Y. Gogotsi, R. Cingolani, *Carbon* **2016**, *109*, 331.
 [38] P. Cataldi, L. Ceseracciu, A. Athanassiou, I. S. Bayer, *ACS Appl. Mater. Interfaces* **2017**, *9*, 13825.
 [39] I. S. Bayer, *Materials* **2017**, *10*, 748.
 [40] S. Stankovich, D. A. Dikin, G. H. Dommett, K. M. Kohlhaas, E. J. Zimney, E. A. Stach, R. D. Piner, S. T. Nguyen, R. S. Ruoff, *Nature* **2006**, *442*, 282.
 [41] P. Cataldi, L. Ceseracciu, S. Marras, A. Athanassiou, I. S. Bayer, *Appl. Phys. Lett.* **2017**, *110*, 121904.
 [42] P. Cataldi, S. Dussoni, L. Ceseracciu, M. Maggiali, L. Natale, G. Metta, A. Athanassiou, I. S. Bayer, *Adv. Sci.* **2018**, *5*, 2.

- [43] T. N. Do, Y. Visell, *Sci. Rep.* **2017**, 7, 1753.
- [44] B. Deng, P.-C. Hsu, G. Chen, B. Chandrashekar, L. Liao, Z. Ayitimuda, J. Wu, Y. Guo, L. Lin, Y. Zhou, M. Aisijiang, Q. Xie, Y. Cui, Z. Liu, H. Peng, *Nano Lett.* **2015**, 15, 4206.
- [45] O.-S. Kwon, H. Kim, H. Ko, J. Lee, B. Lee, C.-H. Jung, J.-H. Choi, K. Shin, *Carbon* **2013**, 58, 116.
- [46] D.-Y. Cho, K. Eun, S.-H. Choa, H.-K. Kim, *Carbon* **2014**, 66, 530.
- [47] R. P. Tortorich, E. Song, J.-W. Choi, *J. Electrochem. Soc.* **2014**, 161, B3044.
- [48] B. Muhsin, R. Roesch, G. Gobsch, H. Hoppe, *Sol. Energy Mater. Sol. Cells* **2014**, 130, 551.
- [49] K. Devarayan, D. Lei, H.-Y. Kim, B.-S. Kim, *Chem. Eng. J.* **2015**, 273, 603.
- [50] R. Kurapati, J. Russier, M. A. Squillaci, E. Treossi, C. Ménard-Moyon, D. Rio-Castillo, A. Esaú, E. Vazquez, P. Samor, V. Palermo, A. Bianco, *Small* **2015**, 11, 3985.
- [51] W. Xing, G. Lalwani, I. Ruskova, B. Sitharaman, *Part. Part. Syst. Charact.* **2014**, 31, 745.
- [52] A. Morfa, T. Rödlmeier, N. Jürgensen, S. Stolz, G. Hernandez-Sosa, *Cellulose* **2016**, 23, 3809.
- [53] P. Saini, M. Arora, *New Polymers for Special Applications*, InTech, London **2012**.
- [54] J.-M. Thomassin, C. Jerome, T. Pardoën, C. Bailly, I. Huynen, C. Detrembleur, *Mater. Sci. Eng.: Rep.* **2013**, 74, 211.
- [55] L. Liu, A. Das, C. M. Megaridis, *Carbon* **2014**, 691.
- [56] J. E. Mates, I. S. Bayer, M. Salerno, P. J. Carroll, Z. Jiang, L. Liu, C. M. Megaridis, *Carbon* **2015**, 87, 163.
- [57] B. Sensale-Rodriguez, R. Yan, L. Liu, D. Jena, H. G. Xing, *Proc. IEEE* **2013**, 101, 1705.
- [58] B. Sensale-Rodriguez, R. Yan, S. Rafique, M. Zhu, W. Li, X. Liang, D. Gundlach, V. Protasenko, M. M. Kelly, D. Jena, L. Liu, H. G. Xing, *Nano Lett.* **2012**, 12, 4518.
- [59] A. Das, C. M. Megaridis, L. Liu, T. Wang, A. Biswas, *Appl. Phys. Lett.* **2011**, 98, 174101.
- [60] D.-X. Yan, P.-G. Ren, H. Pang, Q. Fu, M.-B. Yang, Z.-M. Li, *J. Mater. Chem.* **2012**, 22, 18772.
- [61] T. Inui, H. Koga, M. Nogi, N. Komoda, K. Suganuma, *Adv. Mater.* **2015**, 27, 1112.
- [62] X. Huang, T. Leng, K. H. Chang, J. C. Chen, K. S. Novoselov, Z. Hu, *2D Mater.* **2016**, 3, 025021.
- [63] A. Scidà, S. Haque, E. Treossi, A. Robinson, S. Smerzi, S. Ravesi, S. Borini, V. Palermo, *Mater. Today* **2018**, 21, 223.
- [64] P. Froehle, T. Przybylski, C. McDonald, M. Mirzaee, S. Noghianian, R. Fazel-Rezai, *2015 IEEE Int. Symp. on Antennas and Propagation & USNC/URSI National Radio Science Meeting*, IEEE, USA **2015**, pp. 1214–1215.
- [65] J. J. Adams, E. B. Duoss, T. F. Malkowski, M. J. Motala, B. Y. Ahn, R. G. Nuzzo, J. T. Bernhard, J. A. Lewis, *Adv. Mater.* **2011**, 23, 1335.
- [66] J.-H. So, J. Thelen, A. Qusba, G. J. Hayes, G. Lazzi, M. D. Dickey, *Adv. Funct. Mater.* **2009**, 19, 3632.
- [67] M. Kubo, X. Li, C. Kim, M. Hashimoto, B. J. Wiley, D. Ham, G. M. Whitesides, *Adv. Mater.* **2010**, 22, 2749.
- [68] D. M. Pozar, *Microwave Engineering*, 4th ed., Wiley, Weinheim, Germany **2012**.
- [69] S. C. Satapathy, N. B. Rao, S. S. Kumar, C. D. Raj, V. M. Rao, G. Sarma, *Microelectronics, Electromagnetics and Telecommunications: Proceedings of ICMEET 2015*, Vol. 372, Springer, USA **2015**.
- [70] V. Pranavses, P. Jain, *2016 Int. Conf. on Computational Techniques in Information and Communication Technologies (ICCTICT)*, IEEE, USA **2016**, pp. 575–579.
- [71] C. A. Balanis, *Antenna Theory: Analysis and Design*, John Wiley and Sons Inc., USA **2005**.
- [72] http://www.molex.com/molex/products/datasheet.jsp?part=active/0479502011_ANTENNAS.xml&channel=Products&Lang=en-US, (accessed: March 2018).
- [73] M. Akbari, M. W. A. Khan, M. Hasani, T. Björninen, L. Sydänheimo, L. Ukkonen, *IEEE Antennas Wireless Propag. Lett.* **2016**, 15, 1569.
- [74] X. Huang, T. Leng, M. Zhu, X. Zhang, J. Chen, K. Chang, M. Aqeeli, A. K. Geim, K. S. Novoselov, Z. Hu, *Sci. Rep.* **2015**, 5, 18298.
- [75] M. R. Wasielewski, *J. Org. Chem.* **2006**, 71, 5051.
- [76] P. Löper, B. Niesen, S.-J. Moon, S. M. De Nicolas, J. Holovsky, Z. Remes, M. Ledinsky, F.-J. Haug, J.-H. Yum, S. De Wolf, C. Ballif, *IEEE J. Photovoltaics* **2014**, 4, 1545.
- [77] E. Klugmann-Radziemska, P. Ostrowski, *Renewable Energy* **2010**, 35, 1751.
- [78] S. Kang, S. Yoo, J. Lee, B. Boo, H. Ryu, *Renewable Energy* **2012**, 47, 152.
- [79] L. La Notte, P. Cataldi, L. Ceseracciu, I. S. Bayer, A. Athanassiou, S. Marras, E. Villari, F. Brunetti, A. Reale, *Mater. Today Energy* **2018**, 7, 105.
- [80] L. La Notte, G. Polino, C. Ciceroni, F. Brunetti, T. M. Brown, A. Di Carlo, A. Reale, *Energy Technol.* **2014**, 2, 9.
- [81] A. Reale, L. La Notte, L. Salamandra, G. Polino, G. Susanna, T. M. Brown, F. Brunetti, A. Di Carlo, *Energy Technol.* **2015**, 3, 385.
- [82] L. La Notte, G. V. Bianco, A. L. Palma, A. Di Carlo, G. Bruno, A. Reale, *Carbon* **2018**, 129, 878.
- [83] L. La Notte, D. Mineo, G. Polino, G. Susanna, F. Brunetti, T. M. Brown, A. Di Carlo, A. Reale, *Energy Technol.* **2013**, 1, 757.
- [84] Y. Zhou, C. Fuentes-Hernandez, T. M. Khan, J.-C. Liu, J. Hsu, J. W. Shim, A. Dindar, J. P. Youngblood, R. J. Moon, B. Kippelen, *Sci. Rep.* **2013**, 3, 1536.
- [85] F. C. Krebs, N. Espinosa, M. Hösel, R. R. Søndergaard, M. Jørgensen, *Adv. Mater.* **2014**, 26, 29.
- [86] R. Po, A. Bernardi, A. Calabrese, C. Carbonera, G. Corso, A. Pellegrino, *Energy Environ. Sci.* **2014**, 7, 925.
- [87] Y. Liu, J. Zhao, Z. Li, C. Mu, W. Ma, H. Hu, K. Jiang, H. Lin, H. Ade, H. Yan, *Nat. Commun.* **2014**, 5, 5293.
- [88] Y.-C. Huang, C.-W. Chou, D.-H. Lu, C.-Y. Chen, C.-S. Tsao, *IEEE J. Photovoltaics* **2017**, 8, 144.
- [89] S. Arumugam, Y. Li, S. Senthilarasu, R. Torah, A. Kanibolotsky, A. Inigo, P. Skabara, S. Beeby, *J. Mater. Chem. A* **2016**, 4, 5561.
- [90] M. Tosin, M. Weber, M. Siotto, C. Lott, F. Degli Innocenti, *Front. Microbiol.* **2012**, 3, 225.
- [91] P. Pieranski, J. Baranska, A. Skjeltorp, *Eur. J. Phys.* **2004**, 25, 613.
- [92] M. A. Berger, C. Prior, *J. Phys. A: Math. Gen.* **2006**, 39, 8321.
- [93] M. Duocastella, C. B. Arnold, *Laser Photonics Rev.* **2012**, 6, 607.